The Journal of Chemical Physics

RESEARCH ARTICLE | APRIL 14 2026

Nuclear–electronic orbital quasiclassical trajectory method for vibrational spectroscopy

Special Collection: Computational Spectroscopy

Chiara Aieta ; Scott M. Garner ; Aodong Liu ; Xiaosong Li ; Sharon Hammes-Schiffer

J. Chem. Phys. 164, 144123 (2026)
https://doi.org/10.1063/5.0317500

The Journal of Chemical Physics ARTICLE pubs.aip.org/aip/jcp

Nuclear–electronic orbital quasiclassical trajectory method for vibrational spectroscopy

Cite as: J. Chem. Phys. 164, 144123 (2026); doi: 10.1063/5.0317500
Submitted: 18 December 2025 • Accepted: 5 February 2026 •
Published Online: 14 April 2026

Chiara Aieta,[1,2] Scott M. Garner,[1] Aodong Liu,[3] Xiaosong Li,[3,a)] and Sharon Hammes-Schiffer[1,b)]

AFFILIATIONS

[1] Department of Chemistry, Princeton University, Princeton, New Jersey 08544, USA
[2] Dipartimento di Chimica, Università degli Studi di Milano, Milano 20133, Italy
[3] Department of Chemistry, University of Washington, Seattle, Washington 98195, USA

Note: This paper is part of the Special Topic on Computational Spectroscopy.
[a)]**Electronic mail:** xsli@uw.edu
[b)]**Author to whom correspondence should be addressed:** shs566@princeton.edu

ABSTRACT

Simulations of vibrational spectra are important for interpreting experimental data as well as understanding molecular structure and dynamics. Herein, we present an approach for the efficient and accurate incorporation of anharmonicity into such simulations. Real-time nuclear–electronic orbital time-dependent density functional theory treats specified protons quantum mechanically on the same level as the electrons, propagating the electronic and protonic densities according to the time-dependent Schrödinger equation. This approach inherently includes the anharmonicity of the quantum protons and can be combined with Ehrenfest dynamics for the classical nuclei. Herein, this real-time nuclear–electronic orbital (NEO)–Ehrenfest approach is combined with the quasiclassical trajectory (QCT) approach for generating initial conditions that include the zero-point energy of the classical nuclei, thereby enabling sampling of the anharmonic regions of the potential energy surface. The resulting NEO-QCT approach is shown to capture the anharmonic heavy nuclear motion, as well as the anharmonicity of the quantum protons, for a series of molecular systems, including HCN, HNC, FHF^-, CH_2O, and HCOOH. The NEO-QCT method also captures the distinct spectral features of the formate–water complex ($CHO_2^- \cdot H_2O$), including the redshifted and broadened OH stretch band due to strong anharmonicity arising from hydrogen bonding and coupling between the motions of the hydrogen nuclei and the heavy nuclei. The NEO-QCT method enables computationally practical simulations of vibrational spectra of molecules that exhibit significant anharmonicity and coupling between vibrational modes.

I. INTRODUCTION

Vibrational spectroscopy is a cornerstone of understanding chemical and biological systems. Spectroscopy is inherently a quantum mechanical process, as it is related to transitions between quantum mechanical vibrational levels induced or stimulated by the interaction with light. Nevertheless, a typical approach for simulating vibrational spectra is to use classical molecular dynamics (MD) without explicitly including nuclear quantum effects. Such approaches yield results comparable with experimental data for molecular systems that are predominantly harmonic or for condensed phase systems in specific cases when the nuclear quantum effects are averaged out.[1,2]

However, nuclear quantum effects (NQEs) are often associated with spectral features that cannot be captured with classical simulations.[3–5] The neglect of NQEs such as nuclear delocalization, zero-point energy (ZPE), and tunneling in classical MD simulations can limit the accuracy of both the frequencies and intensities of vibrational spectral features. When vibrations exhibit a high degree of anharmonicity, the inclusion of NQEs, such as nuclear delocalization and ZPE, to enable sampling of the anharmonic region of the potential energy surface is necessary to predict the correct frequencies. Due to the neglect of NQEs, classical MD simulations usually exhibit blueshifted spectral features compared to exact quantum dynamical calculations or experiments.[3] Significant NQEs are also observed for the intensities of the overtones and combination

bands.[4] Another shortcoming of classical MD is the underestimation of the mode mixing in Fermi resonances.[4,6] Finally, tunneling is responsible for the splittings of signals in the vibrational spectra of some systems, and tunneling cannot be described by classical MD.

Simulating vibrational spectra at the fully quantum mechanical level requires numerically exact quantum approaches that typically scale exponentially with the number of degrees of freedom. Examples of fully quantum mechanical approaches are the vibrational configuration interaction (VCI) method,[7,8] the second-order vibrational perturbation theory (VPT2) method,[9,10] and the multiconfiguration time-dependent Hartree (MCTDH) method.[11,12] To mitigate the unfavorable scaling of fully quantum mechanical calculations, several trajectory-based methods have been devised. Path integral methods can be divided into imaginary-time-based techniques,[3,13] such as ring-polymer molecular dynamics (RPMD),[14] centroid molecular dynamics (CMD),[15] and real-time methods, such as the semiclassical initial value representation (SC-IVR) approaches.[5,16–22] These trajectory-based methods approximately include NQEs from all the nuclei in the system by taking advantage of the linear scaling with the number of degrees of freedom of classical trajectory simulations. Different approximations can capture the NQEs to various extents.[3,4]

A different class of methods is based on the hypothesis that the most significant NQEs in molecular systems are associated with specific nuclei, such as the lighter hydrogens. Therefore, an effective way to fight the unfavorable scaling of fully quantum calculations is to treat only specified nuclei at the quantum level, while describing the remaining nuclei at the classical level. This premise underlies most implementations of the nuclear electronic orbital (NEO) approach.[23–25] The NEO approach is a multicomponent quantum chemistry method, where selected nuclei are treated on the same footing as the electrons, while the remaining nuclei are treated as classical point charges, as in conventional electronic structure calculations. The NEO approach provides vibronic energy levels for the quantum subsystem composed of protons and electrons, including non-Born–Oppenheimer effects. A wide range of NEO methods have been developed over the years, including NEO Hartree–Fock theory (NEO-HF),[23] NEO density functional theory (NEO-DFT),[26–28] NEO time-dependent DFT (NEO-TDDFT),[29,30] NEO configuration interaction (NEO-CI) and multireference CI (NEO-MRCI),[23,31,32] and NEO coupled cluster theory (NEO-CC).[33]

As the NEO potential energy surface depends on only the coordinates of the classical nuclei, the NEO vibronic energy levels are not directly comparable with vibrational spectroscopy experiments. The NEO vibrational [NEO(V)][34,35] and constrained NEO (CNEO)[36,37] approaches address this issue in a practical manner. In the NEO(V) approach, the NEO Hessian, given by the second derivatives of the NEO energy with respect to the classical nuclei, is extended by using the second derivatives of the NEO energy with respect to the position expectation values of the quantum nuclei to recover the full molecular dimensionality. The vibrational frequencies are calculated by diagonalizing this extended NEO Hessian. Along the same lines, the CNEO approach constructs an extended energy surface that depends on the coordinates of the classical nuclei and the position expectation values of the quantum nuclei. The CNEO potential energy surface is obtained by constraining the position expectation value of the quantum nuclear position operator. Since the CNEO potential energy surface has a dimensionality corresponding to that of a conventional electronic surface, a classical MD trajectory can be propagated to calculate the correlation functions required to simulate vibrational spectra.[38–41]

An alternative approach for computing vibrational spectra is to combine the real-time NEO-TDDFT (RT-NEO) method[42] with Ehrenfest dynamics.[43,44] The RT-NEO method propagates the electronic and protonic densities numerically according to the time-dependent Schrödinger equation.[42] An advantage of the RT-NEO–Ehrenfest approach is that it accounts for the feedback between the classical nuclei and the electron–proton quantum subsystem via Ehrenfest dynamics. This approach has been shown to produce accurate vibrational spectra for small molecules.[43]

In this work, we demonstrate how the RT-NEO–Ehrenfest approach can yield accurate vibrational spectra that align with experimental measurements. Particular attention is devoted to the choice of initial conditions. In particular, we employ a quasiclassical trajectory (QCT) approach to account for the ZPE of the classical subsystem. We demonstrate how this implementation improves on previous results for triatomic molecules with a single quantum proton.[43] We also show that this approach effectively treats more complex anharmonic molecular systems.

This paper is organized as follows: Section II summarizes the RT-NEO–Ehrenfest approach, the calculation of vibrational spectra from the total dipole moment of a molecular system, and the generation of the QCT initial conditions. Section III provides the computational details for the simulations. Section IV presents the results for simple linear molecules, formic acid, and the more challenging formate–water complex. Section V summarizes the results and discusses future directions.

II. METHODS

A. NEO–Ehrenfest algorithm

In this subsection, we provide a brief review of the RT-NEO–Ehrenfest algorithm used in this paper. More details can be found in the original paper.[43]

In the RT-NEO–Ehrenfest approach, the NEO multicomponent Hamiltonian is

$$\hat{H}_{\mathrm{NEO}} = \hat{T}_{\mathrm{e}} + \hat{T}_{\mathrm{p}} + \hat{V}_{\mathrm{ee}} + \hat{V}_{\mathrm{pp}} + \hat{V}_{\mathrm{ep}} + \hat{V}_{\mathrm{ec}} + \hat{V}_{\mathrm{pc}}. \tag{1}$$

This Hamiltonian includes the proton kinetic energy, $\hat{T}_{\mathrm{p}}$, and the Coulomb terms involving the proton–proton, $\hat{V}_{\mathrm{pp}}$, electron–proton, $\hat{V}_{\mathrm{ep}}$, and proton–classical nucleus, $\hat{V}_{\mathrm{pc}}$, interactions, as well as the analogous conventional electronic terms. The dynamics of the classical nuclei follow Newton's equations of motion with a mean-field potential generated by the electronic–protonic wavefunction $|\Phi\rangle$. The equations of motion are

$$i\hbar\frac{\partial|\Phi\rangle}{\partial t} = \hat{H}_{\mathrm{NEO}}|\Phi\rangle, \tag{2}$$

$$M_I\ddot{\boldsymbol{R}}_I = -\nabla_I\langle\Phi|\hat{H}_{\mathrm{NEO}}|\Phi\rangle - \nabla_I V_{\mathrm{cc}}, \tag{3}$$

where $\hbar$ is the reduced Planck's constant, V_{cc} is the Coulomb interaction between the classical nuclei, and the index I denotes the classical nucleus of mass M_I and coordinates $\boldsymbol{R}_I$.

In this paper, we employ the NEO-DFT[26–28] and NEO-TDDFT[29,30] levels of theory. The propagation of the electronic–protonic subsystem of Eq. (2) is performed with the RT-NEO-TDDFT method,[42] which propagates two coupled von Neumann equations,

$$i\hbar\frac{\partial}{\partial t}\boldsymbol{P}^{\mathrm{e}}(t) = \left[\boldsymbol{F}^{\mathrm{e}}\left(t,\boldsymbol{P}^{\mathrm{e}}(t),\boldsymbol{P}^{\mathrm{p}}(t)\right),\boldsymbol{P}^{\mathrm{e}}(t)\right],$$
$$i\hbar\frac{\partial}{\partial t}\boldsymbol{P}^{\mathrm{p}}(t) = \left[\boldsymbol{F}^{\mathrm{p}}\left(t,\boldsymbol{P}^{\mathrm{p}}(t),\boldsymbol{P}^{\mathrm{e}}(t)\right),\boldsymbol{P}^{\mathrm{p}}(t)\right]. \tag{4}$$

Here, $\boldsymbol{F}^{\mathrm{e}}$ and $\boldsymbol{F}^{\mathrm{p}}$ are the electronic and protonic Fock matrices, respectively, and $\boldsymbol{P}^{\mathrm{e}}$ and $\boldsymbol{P}^{\mathrm{p}}$ are the electronic and protonic density matrices, respectively, represented in the orthogonal atomic orbital basis. If the excited electronic states are not relevant to the process, the electronic Born–Oppenheimer approximation can be employed to reduce the computational cost of the real-time propagation.[45] With this approach, the electronic density is quenched to the electronic ground state at each time step during the evolution, allowing for larger time steps, thereby reducing the overall computational cost.

To alleviate the requirement of a large basis set for describing proton motion during dynamics, we employ a traveling proton basis (TPB) approach. Among the several schemes available,[43,46,47] we evolve the Q-th electronic and protonic basis function centers associated with the quantum protons according to a classical dynamics equation of motion,

$$m_{\mathrm{p}}\ddot{\boldsymbol{\mathcal{R}}}_Q = -\nabla_Q\langle\Phi|\hat{H}_{\mathrm{NEO}}|\Phi\rangle, \tag{5}$$

where the mass m_{p} is selected to be the proton mass and the energy gradient is taken with respect to the proton basis function center coordinates $\boldsymbol{\mathcal{R}}_Q$. This scheme was proposed in previous work and demonstrated to be beneficial in enhancing the accuracy of vibrational frequencies for selected small molecules compared to a fixed basis approach.[43] We note that this TPB scheme does not conserve the energy of the system but does conserve the energy of the extended system, which includes the kinetic energy of the basis function centers, based on an extended Lagrangian.[46] With this specific propagation scheme, reliable dynamics for bound potentials, such as those of interest in vibrational spectroscopy, can be obtained, as demonstrated for model systems where the numerically exact dynamics can be propagated.[44]

B. Calculation of vibrational spectra

In our simulations, the time-dependent dipole can be computed from the time evolution of the electronic and protonic densities. The contribution from the dynamics of the classical nuclei is included by adding the dipole moment associated with the classical nuclei, $\boldsymbol{\mu}^{\mathrm{c}}$, to the dipole moment of the quantum subsystem, $\boldsymbol{\mu}(t)$,

$$\boldsymbol{\mu}^{\mathrm{tot}}(t) = \boldsymbol{\mu}(t) + \boldsymbol{\mu}^{\mathrm{c}}(t) = \boldsymbol{\mu}(t) + \sum_{i=1}^{N_{\mathrm{c}}} Z_i\boldsymbol{R}_i(t). \tag{6}$$

Here N_{c} is the number of classical nuclei, and Z_i and $\boldsymbol{R}_i$ are their charges and position coordinates, respectively.

To obtain spectra that can be compared with experiments, we employ the power spectrum $I(\omega)$ computed from the time-evolved total dipole moment,[48,49]

$$I(\omega) \propto \omega\left|\int_0^{t_{\max}}\left(\boldsymbol{\mu}^{\mathrm{tot}}(t) - \boldsymbol{\mu}^{\mathrm{tot}}(0)\right)e^{i\omega t}e^{-\Gamma t}dt\right|^2, \tag{7}$$

where $t_{\max}$ is the total simulation time. The Fourier transform of the time-dependent dipole moment, as given in Eq. (7), is performed using an additional damping term $e^{-\Gamma t}$ to obtain a Lorentzian line shape with a width determined by Γ. A specific Γ value has been selected for the different spectra and will be reported for each case.

C. General considerations for initial conditions

To initialize the dynamics, several different strategies have been used in previous work. Starting at the NEO ground state equilibrium geometry, the electronic–protonic wavefunction can be perturbed by orbital swapping to simulate a photoexcited reaction.[44] Another possibility, if the vibrational motion is the main interest, is to perturb the initial geometry by a small distortion. This strategy, which we denote NEO-$\delta_{\mathbf{R}}$, was employed to estimate the vibrational frequencies of small molecules containing a single quantum proton.[43]

In this work, we devise a protocol for initializing the NEO–Ehrenfest dynamics using the quasiclassical trajectory (QCT) approach. The objective of this protocol is to simulate vibrational spectra with improved accuracy, thereby allowing applications to more complex cases of highly anharmonic systems. An aspect that will be improved is the description of the dynamics of the classical nuclei, which are coupled to the electronic–protonic quantum subsystem. A NEO–Ehrenfest dynamics simulation takes into account the anharmonic ZPE of the quantum mechanical protons but overlooks the quantum nature of the other nuclei. Our goal is to devise a strategy to account for contributions from the ZPE associated with the other nuclei in an approximate manner. By including the ZPE for the classical subsystem, the Ehrenfest trajectory explores higher-energy regions of the potential energy surface, thereby allowing the anharmonicity of the overall system to be more accurately captured.

The problem of finding vibrational eigenvalues, and thus the ZPE, using classical trajectories has a long history, tracing back to the Einstein, Brillouin, and Keller (EBK) quantization rules.[50,51] The QCT approach establishes a correspondence between classical trajectories and quantum states. This technique is well-known for reaction rate constant calculations, where the vibrational quantum states of the reactant molecules are approximated with an ensemble of classical states.[52,53] In particular, normal mode sampling is used to generate classical states corresponding to the quantum vibrational states. This method has also been used for molecular vibrational spectroscopy to enhance the accuracy of classical MD simulations.[54–57]

The QCT approach includes the nuclear ZPE and accounts for the quantum distribution of energy across the nuclear degrees of freedom. However, since the dynamics still evolve classically, the system will redistribute its energy over time to reach the classical equipartition. Due to this energy redistribution, some of the modes can have less energy than the ZPE at later times during the dynamics. This issue is known as the ZPE leakage and is alleviated by

propagating trajectories that are not too long in time.[58–60] Thus, a trajectory must be short enough to prevent the energy leakage problem but long enough to allow all the modes to vibrate for at least one cycle and have enough points for sufficient resolution of the spectrum after the Fourier transform. We adopted the Padé signal processing[49,61] to treat the short dynamics in this work.

D. NEO-QCT approach

The preparation of the initial state for a molecule in a QCT simulation is achieved through normal mode sampling. The vibrational state of a non-linear (linear) molecule composed of N atoms, regarding rotation and translation separately, is described by $3N-6$ (5) quantum numbers n_i. If the molecule were harmonic, the EBK quantization rule would be exact and is

$$\sum_i \left(\frac{1}{2}p_i^2 + \frac{1}{2}\omega_i^2 q_i^2\right) = \sum_i \left(\frac{1}{2} + n_i\right)\hbar\omega_i, \tag{8}$$

where p_i, q_i, and ω_i are the momenta, positions, and frequencies, respectively, of the normal modes. Equating the corresponding terms on each side of this expression can be used to partition the energy, such that each normal mode is associated with a quantum harmonic oscillator. When each mode undergoes a periodic motion, as in the case of a vibrating molecule, the EBK quantization is still exact even if the potential energy surface is anharmonic. In this case, the quantization rule becomes

$$\sum_i \frac{1}{2}p_i^2 + V(\boldsymbol{q}) = \sum_i \left(\frac{1}{2} + n_i\right)\hbar\ \Xi_i(E), \tag{9}$$

where $\Xi_i(E)$ represent the classical frequencies associated with the periodic motion of each mode. These frequencies depend on the total energy due to the anharmonicity of the potential $V(\boldsymbol{q})$, which is, in general, non-separable. If the energy dependence of the anharmonic frequency is moderate, the harmonic EBK quantization is a good approximation. To improve the accuracy by employing anharmonic initial conditions, adiabatic switching techniques have been proposed.[54,62–64]

When the QCT approach is used to generate initial conditions for dynamics, the harmonic initial conditions are usually sufficient, as the evolution of the dynamics ensures exploration of the anharmonic region of the potential energy surface. In this case, the quantization of the trajectory is achieved by selecting the conditions for the initial step of the dynamics as follows:

$$\begin{aligned} q_i(t=0) &= 0, \\ p_i(t=0) &= \sqrt{(1+2n_i)\hbar\omega_i}. \end{aligned} \tag{10}$$

These initial conditions assume that the molecule is in its equilibrium geometry. However, a random phase γ_i, which is selected from a uniform distribution in the range $[0, 2\pi]$, can be added to partition the starting energy of the i-th normal mode into potential and kinetic energy terms. The initial conditions become

$$\begin{aligned} q_i(t=0) &= \sqrt{\frac{(1+2n_i)\hbar}{\omega_i}}\sin(\gamma_i), \\ p_i(t=0) &= \sqrt{(1+2n_i)\hbar\omega_i}\cos(\gamma_i). \end{aligned} \tag{11}$$

In this work, we choose to use the single initial condition of Eq. (10), rather than propagating multiple trajectories with different initial conditions using Eq. (11), to show that reliable vibrational spectra can be obtained with a single trajectory, which will be more practical for larger molecular systems.

This procedure is based on the knowledge of the normal mode frequencies and eigenvectors. To apply this approach to the classical subsystem composed of N_c classical nuclei in a NEO–Ehrenfest calculation, we rely on the Hessian at the minimum energy geometry on the NEO ground state. In this case, we have a total of $3N_c-6$ ($3N_c-5$ if the classical nuclei are linear) normal modes, with the corresponding frequencies ω_i^{NEO} to be used in Eqs. (10) or (11). Since our objective in this work is to include the ZPE of the classical subsystem in the NEO–Ehrenfest dynamics, we select all the quantum number values as $n_i = 0$, and our initial conditions are

$$\begin{aligned} q_i(t=0) &= 0, \\ p_i(t=0) &= \sqrt{\hbar\omega_i^{\mathrm{NEO}}}, \end{aligned} \tag{12}$$

where $q_i = 0$ corresponds to the equilibrium geometry. Finally, we convert the normal mode velocities to Cartesian velocities using the conversion matrix that diagonalizes the NEO Hessian because the dynamics will be evolved in Cartesian coordinates.

For numerical reasons, we find that the frequencies related to rotations are not exactly zero. This issue contaminates the initial Cartesian velocities with rotational contributions, which might build up during the dynamics. To correct for this issue, we use a simple initial velocity rescaling approach. We subtract from each nuclear Cartesian velocity the components that contribute to the total molecular angular momentum, obtaining a modified set of velocities $\tilde{\boldsymbol{v}}$. The total energy, $\tilde{E} = \sum_i \frac{1}{2}m_i\tilde{v}_i^2$, is now lower than the original target energy, E_{ZPE}, which corresponds to the ZPE associated with the classical subsystem. We then scale the modified velocities $\tilde{\boldsymbol{v}}$ to obtain the velocities $\boldsymbol{v}$ that restore the original target energy, E_{ZPE}, such that

$$v_i = \tilde{v}_i\sqrt{\frac{E_{\mathrm{ZPE}}}{\tilde{E}}} \tag{13}$$

and

$$\sum_i \frac{1}{2}m_i v_i^2 = \frac{E_{\mathrm{ZPE}}}{\tilde{E}}\sum_i \frac{1}{2}m_i\tilde{v}_i^2 = E_{\mathrm{ZPE}}. \tag{14}$$

III. COMPUTATIONAL DETAILS

To perform the simulations, we first prepared geometries and initial velocities for the classical nuclei using Q-Chem 6.3 software.[65] We started by performing a NEO-DFT geometry optimization. For HCN, HNC, FHF^-, and H_2CO, we used the B3LYP electronic functional.[66] For the formate–water complex, we tested three electronic functionals: B3LYP, PBE0,[67] and ωB97X.[68] For HCN, HNC, FHF^-, and H_2CO, we used the cc-pVDZ electronic basis set for the non-hydrogen atoms and the cc-pV5Z electronic basis set for the hydrogen atoms.[69] For HCOOH, we used the cc-pVTZ electronic basis set for all atoms. For the formate–water complex, we used the cc-pVTZ electronic basis set for the non-hydrogen atoms and the

cc-pV5Z electronic basis set for the hydrogen atoms. For all systems, we used the epc17-2 electron–proton correlation functional[27,28] and the PB4-F2 protonic basis set.[70] Both electronic and protonic basis sets were used in their spherical coordinate form. To obtain reliable geometries and NEO Hessians, we specified tight thresholds for both the self-consistent field (SCF) procedure and the geometry optimization. The harmonic frequencies and second-order vibrational perturbation theory (VPT2) calculations serving as references were computed at the same level of theory as the electronic portion of the NEO calculations. All input files are available in Zenodo.

The NEO–Ehrenfest dynamics simulations were performed using the Chronus Quantum open-source package.[71] To start the dynamics, we first calculated the electronic–protonic wavefunction at the previously optimized geometry. The initial protonic one-particle density matrix was produced by occupying the tightest orbital(s), and the electronic one-particle density matrix was obtained from a conventional SCF calculation. The SCF DIIS algorithm was employed,[72] and the convergence was determined to be achieved when the difference in energy between consecutive iterations was less than 10^{-10} a.u., the maximum density difference was less than 10^{-10} a.u., and the root-mean-square density difference was less than 10^{-12} a.u.

Following the approach introduced by Li *et al.*,[73] we performed the Ehrenfest dynamics simulations using a triple-split time step: we used the largest time step $\Delta t_{N_g} = 0.1$ fs to compute the energy gradients, an intermediate time step $\Delta t_{N_c} = 0.01$ fs to update the position coordinates of the classical nuclei evolved with the velocity Verlet integrator, and the smallest time step $\Delta t_{N_q} = 0.001$ fs to perform the real-time propagation of the electronic and protonic density matrices using a modified midpoint unitary transform (MMUT) propagator.[74] To reduce the computational cost for the formate–water complex dynamics, we employed the electronic Born–Oppenheimer approximation.[45] With this method, we could use larger time steps of $\Delta t_{N_c} = 0.05$ fs and $\Delta t_{N_q} = 0.01$ fs.

We conducted two types of NEO simulations. For the NEO-$\delta_{\mathbf{R}}$ approach, the initial conditions for starting the Ehrenfest trajectories consisted of a slight distortion of the optimized NEO-DFT geometry. For the NEO-QCT approach, the initial conditions were set according to Eq. (10). For each NEO-$\delta_{\mathbf{R}}$ or NEO-QCT simulation, we propagated a single 200 fs trajectory, with the exception that we propagated 600 fs trajectories for the formate–water complex.

IV. RESULTS

A. Simple molecules

In this section, we begin by examining the impact of QCT initial conditions on molecules with linear heavy-atom geometries. We first focus on three molecules with a single quantum proton: HCN, HNC, and FHF^-. These systems were already simulated with RT-NEO–Ehrenfest dynamics to calculate vibrational frequencies.[43] This previous work used the NEO-$\delta_{\mathbf{R}}$ approach, where one of the terminal heavy atom positions was perturbed by 10^{-5} bohr along the three Cartesian coordinate directions. In Table I, we compare the results of the NEO-$\delta_{\mathbf{R}}$ and NEO-QCT approaches. Second-order vibrational perturbation theory (VPT2) serves as a reference. These VPT2 calculations employed the B3LYP functional and a mixed electronic basis set, cc-pVDZ for non-hydrogen atoms and cc-pV5Z for hydrogen atoms, consistent with the NEO calculations. For all three molecules, the mean absolute error (MAE) is improved with the QCT initial conditions. For HNC, the NEO-$\delta_{\mathbf{R}}$ estimate for the NH bend deviates by only 9 cm^{-1} from the VPT2 reference value, but the NEO-QCT approach provides a better estimate for two out of the three modes. The NEO-QCT approach provides more accurate vibrational frequencies for the modes dominated by the heavy nuclei in all cases. Given the minimal geometry perturbation in the NEO-$\delta_{\mathbf{R}}$ approach, the classical trajectory does not have enough energy to explore the anharmonic region of the potential energy surface for these modes.

TABLE I. Triatomic molecule vibrational frequencies (in cm^{-1}) calculated using RT-NEO-TDDFT–Ehrenfest with the NEO-$\delta_{\mathbf{R}}$ and NEO-QCT approaches. The mean absolute error (MAE) is calculated using the VPT2 frequencies as the reference. The absolute differences of the calculated frequencies compared to the VPT2 reference values are given in parentheses.

	Vibrational mode	Harmonic	Ref. VPT2	NEO-$\delta_{\mathbf{R}}$	NEO-QCT
HCN	CH bend	787	760	866 (106)	859 (99)
	CN stretch	2203	2176	2222 (46)	2180 (4)
	CH stretch	3465	3328	3521 (193)	3431 (103)
			MAE	115	69
HNC	NH bend	457	455	464 (9)	382 (73)
	NC stretch	2104	2068	2097 (29)	2090 (22)
	NH stretch	3825	3626	3791 (165)	3710 (84)
			MAE	68	60
FHF^-	FF stretch	649	593	639 (46)	623 (30)
	FH bend	1387	1350	1451 (101)	1390 (40)
	FH stretch	1762	1725	2114 (389)	2108 (383)
			MAE	179	151

TABLE II. Formaldehyde vibrational frequencies (in cm^{-1}) calculated using RT-NEO-TDDFT–Ehrenfest with the NEO-δ_R and NEO-QCT approaches. The mean absolute error (MAE) is calculated using the VPT2 frequencies as the reference. The absolute differences of the calculated frequencies compared to the VPT2 reference values are given in parentheses.

	Vibrational mode	Harmonic	Ref. VPT2	NEO-δ_R	NEO-QCT
CH_2O	CH_2 wag	1241	1187	1262 (75)	1115 (72)
	CH_2 rock	1280	1247	1295 (48)	1303 (56)
	CH_2 bend	1555	1517	1627 (110)	1534 (17)
	CO stretch	1824	1799	1816 (17)	1827 (28)
	CH_2 symm. stretch	2885	2739	2921 (182)	2894 (155)
	CH_2 asymm. stretch	2940	2749	2942 (193)	2703 (46)
			MAE	104	62

Next, we focus on formaldehyde, CH_2O, as a simple example with two quantum protons. In this case, the oxygen position was displaced by 10^{-5} bohr along the three Cartesian coordinate directions for the NEO-δ_R calculation. The vibrational frequencies calculated with the different methods are compared in Table II. The VPT2 reference values were obtained with the B3LYP functional and a mixed electronic basis set, cc-pVDZ for non-hydrogen atoms and cc-pV5Z for hydrogen atoms, consistent with the NEO calculations. The agreement of both methods with the VPT2 reference is satisfactory, but the MAE for the NEO-QCT approach is lower than that for the NEO-δ_R approach. Thus, the NEO-QCT approach shows a slight improvement for the vibrational frequencies compared to the previous NEO-δ_R implementation for these simple cases.

B. Formic acid

In this section, we investigate formic acid, HCOOH, as an example of a molecule for which the classical nuclei are in a nonlinear geometry. A molecule with three nonlinear classical nuclei has three modes dominated by the motion of the classical nuclei. For this molecule, the experimental gas-phase infrared (IR) spectrum is available from the NIST database.[75] To perform the NEO-δ_R calculations, there is no clear prescription on how to distort the equilibrium geometry. We chose to perturb the carbonyl oxygen position by 10^{-5} bohr along the three Cartesian coordinate directions. The specific distortion chosen as the initial condition in the NEO-δ_R simulations impacts the quality of the results. One of the advantages of the NEO-QCT approach is that the initial conditions are well-defined.

Figure 1 compares the spectra obtained with the two different methods to the experimental spectrum. The overall accuracy of the spectrum is better for the NEO-QCT approach than for the NEO-δ_R approach. The NEO-QCT approach reproduces the relative intensities of the bands more accurately, specifically for the three modes dominated by the classical nuclei (i.e., the OCO bend, C–O stretch, and C=O stretch), although not quantitatively. The NEO-δ_R approach exhibits two intense peaks in the 2000–2500 cm^{-1} region that are not consistent with the experimental spectrum.

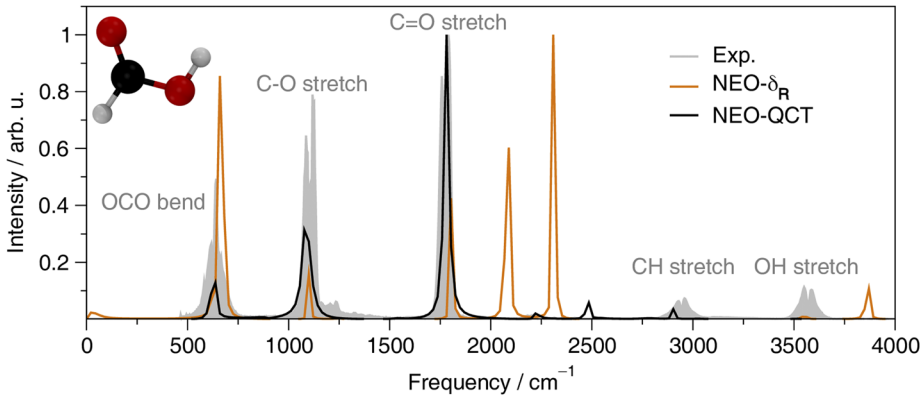

FIG. 1. Comparison of the calculated and experimental formic acid IR spectrum. The gray trace is the experimental spectrum in the gas phase from the NIST database,[75] and the gray labels indicate the experimental band assignment.[76] The black line is the NEO-QCT spectrum, and the orange line is the NEO-δ_R spectrum. The NEO-δ_R and NEO-QCT trajectories were each 200 fs, and a damping factor of $\Gamma = 1.0 \times 10^{-5}$ a.u. was used for the Fourier transform in Eq. (7). All spectra were scaled such that the intensity of the highest peak in each spectrum is set to one.

C. Formate–water complex

The previous examples have focused on the fundamental bands in the vibrational spectra of predominantly harmonic molecules. A more demanding test for our method is a molecule exhibiting significant anharmonicity involving both the classical and quantum nuclei. A type of molecular system with this characteristic is a dimer composed of a molecular anion and a water molecule. This type of system has been extensively studied both experimentally and theoretically.[77–82] Gas phase experimental spectra are available, enabling a direct comparison between the simulated and experimental spectra. A common characteristic of the IR spectra of these dimers is an extreme broadening with a pronounced substructure in the OH stretch region, which reflects the strong anharmonicity and coupling to low-frequency intermolecular modes that involve all the nuclei. The center of this band is also significantly redshifted with respect to the frequency of the harmonic OH stretch. To explain this effect, vibrational adiabatic models have been developed. Static and dynamical approaches have demonstrated that good agreement with experiment is obtained using multidimensional approaches.[81–83] Thus, high-dimensional quantum dynamics methods are required to model this spectral broadening.

We focus on the formate–water complex with the chemical formula $HCO_2^- \cdot H_2O$. Before performing the RT-NEO–Ehrenfest dynamics simulations, we conducted a benchmarking study of the level of theory using the linear-response (LR) NEO-TDDFT approach.[29,30] Because LR-NEO-TDDFT does not account for the motion of the classical nuclei, we cannot expect perfect agreement with the experimental frequencies. The results from the benchmarking are reported in the supplementary material. All the results used the same protonic basis set, PB4-F2, and the epc17-2 functional. Figure S1 shows that different electronic functionals yield qualitatively similar protonic excitation energies when using the same electronic basis set. The electronic basis set is the most critical factor that influences the qualitative results, in agreement with previous studies.[30] When employing the B3LYP functional, a large composite electronic basis set (i.e., cc-pV5Z on the protons and cc-pVTZ on the carbons and oxygen) is necessary to obtain satisfactory qualitative agreement with the experimental frequencies. The LR-NEO-TDDFT excitation energies obtained with this basis set are in the best qualitative agreement with the experimental features (Figs. S2–S4). In this case, augmenting the basis set on the classical nuclei has a minimal effect on the protonic states (Fig. S5). From this benchmarking, we selected the B3LYP electronic functional with the composite cc-pVTZ/H:cc-pV5Z electronic basis set.

With this setup, we simulated the spectrum using the NEO-QCT approach. The convergence of the spectral line shape with the total simulation time is shown in Fig. S6. We found that a trajectory of around 600 fs is needed to obtain a signal in the broadband region of the spectrum. Although this is a high-frequency region, the signal results from the high-frequency OH stretch

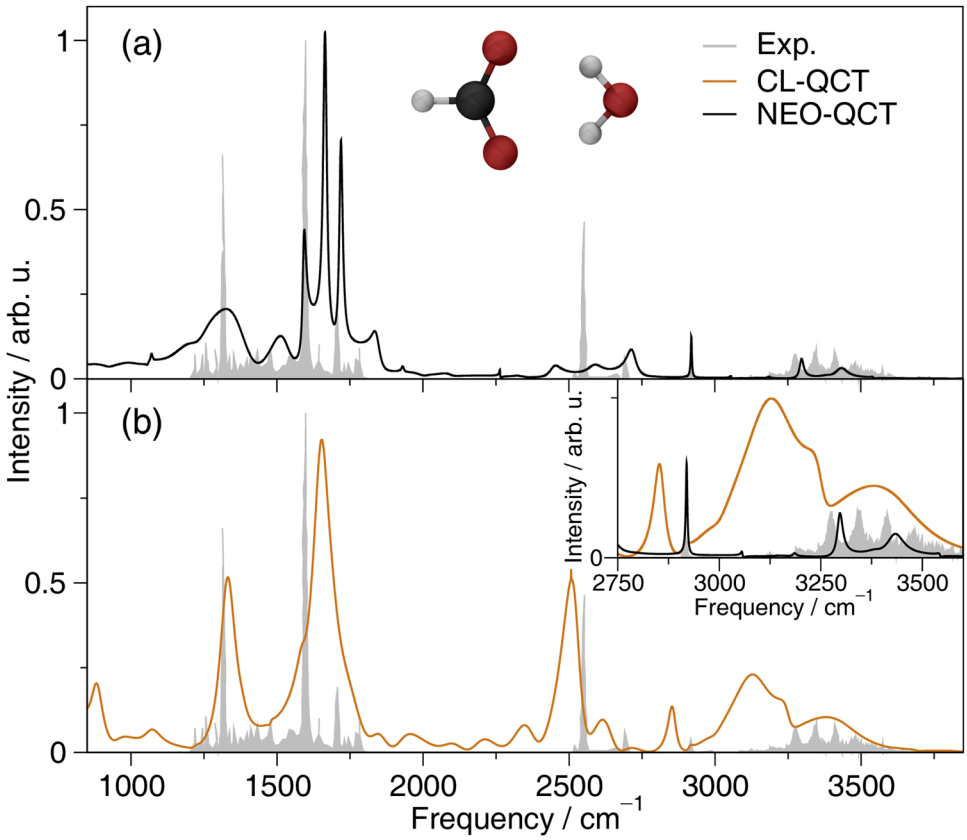

FIG. 2. Comparison of the calculated and experimental formate–water complex IR spectrum. The gray trace indicates the experimental spectrum in the gas phase, digitized from Ref. 77. (a) The black line indicates the NEO-QCT spectrum. (b) The orange line indicates the CL-QCT spectrum. The inset shows a comparison of the CL-QCT and NEO-QCT spectra in the broadband region. The CL-QCT and NEO-QCT trajectories were each 600 fs. For the Fourier transform in Eq. (7), we used a damping factor of $\Gamma = 1.59 \times 10^{-4}$ a.u. for both the NEO-QCT and CL-QCT simulations.

mixing with the low-frequency modes of the dimer. Thus, it is reasonable that we need a longer time to observe the spectral signal arising from this coupling. The disadvantage of propagating for longer times is that the dynamics begin to display numerical instabilities and some spurious features start to appear in the spectrum. We used a damping factor of $\Gamma = 1.59 \times 10^{-4}$ a.u. to remove spurious peaks from the spectrum.

Figure 2(a) shows the spectrum obtained from the NEO-QCT simulation. We applied a 0.95 scaling factor to the frequency axis to align the simulated spectrum with the experimental data, as is common when computing vibrational spectra with DFT.[84] This scaling factor accounts mainly for the limitations of the level of electronic structure theory. For comparison, Fig. 2(b) shows the spectrum obtained from the classical dipole–dipole correlation function computed from a conventional Born–Oppenheimer QCT simulation, denoted CL-QCT, where all the modes were assigned initial harmonic ZPE in the form of kinetic energy. The level of electronic structure theory and the total simulation time for the CL-QCT trajectory were the same as those for the NEO-QCT trajectory, although the scaling factor was not applied. For the CL-QCT spectrum, we used a damping factor of $\Gamma = 1.59 \times 10^{-4}$ a.u.

Both the NEO-QCT and CL-QCT approaches qualitatively reproduce fundamental bands below 2500 cm^{-1}. In this region, the two most intense peaks correspond to modes dominated by the heavy nuclei, namely, the CO symmetric and asymmetric stretches. However, the NEO-QCT approach provides a more accurate substructure in the region around 1700 cm^{-1}. In particular, the NEO-QCT approach resolves the intense peak of the CO asymmetric stretch and the less intense peak related to the water bending at 1707 cm^{-1}, which is dominated by the quantum protons.

The CL-QCT spectrum exhibits an intense feature centered around 3100 cm^{-1}, which can be assigned to the water symmetric and asymmetric stretches (see Fig. S7) but does not appear in the experimental spectrum. This discrepancy arises because the high-frequency OH stretch modes do not mix properly with the low-frequency modes in the classical simulation. In contrast, the NEO-QCT approach describes this mixing properly and the spectrum exhibits intensity only in the broadband region, in agreement with the experimental spectrum [inset of Fig. 2(b)]. Thus, the NEO-QCT approach provides a more accurate description of the coupling between the high- and low-frequency modes.

V. CONCLUSION

This work shows how NEO dynamical calculations can be employed to simulate vibrational spectra for significantly anharmonic molecular systems with multiple quantum protons. The combination of RT-NEO–Ehrenfest dynamics with QCT initial conditions for the classical nuclei is an efficient and accurate approach for computing vibrational spectra. The anharmonic ZPE for the quantum protons is inherently included in the RT-NEO method. The ZPE associated with the other nuclei is incorporated via the QCT initial conditions, ensuring the classical nuclei sample the anharmonic regions of the potential energy surface during the dynamics. The NEO-QCT initial conditions are uniquely defined to within a phase factor based on EBK quantization theory, avoiding arbitrary choices by the user that could impact the spectra. The NEO-QCT approach is applicable to a wide range of other anharmonic molecular systems.[77–82] In addition to computing vibrational spectra, the NEO-QCT approach can be used to simulate nuclear–electronic dynamics of photoinduced processes, such as intramolecular proton transfer.[44]

The NEO-QCT approach provides the foundation for integrating RT-NEO–Ehrenfest dynamics with semiclassical dynamics for the nuclei that are not quantized within the NEO framework. In particular, the multiple-coherent semiclassical initial value representation (MC SC-IVR) approach relies on QCT methods to perform semiclassical simulations of large systems, recovering additional real-time quantum effects while still starting from classical dynamics.[20,85] The combination of the MC SC-IVR approach with the RT-NEO–Ehrenfest approach would offer a practical way to perform dynamical simulations of molecular systems, including quantum effects for all nuclei but at a lower computational cost than a full quantum calculation. These types of hybrid methods will be the subject of future investigations.

SUPPLEMENTARY MATERIAL

The supplementary material is available free of charge: LR-NEO-TDDFT benchmarking for the formate–water complex, convergence of the NEO-QCT simulated spectra with the total simulation time, method used for the assignment of the classical formate–water complex spectrum, and the formic acid Fourier transform spectrum.

ACKNOWLEDGMENTS

C.A. acknowledges the Horizon Europe research and innovation programme for providing funding under the Marie Skłodowska-Curie Grant Agreement No. 101106284. The real-time NEO aspects of this work were also supported by the National Science Foundation under Grant Nos. CHE-2408934 (S.H.-S.) and CHE-2515209 (X.L.). The software infrastructure, including NEO integrals and self-consistent-field, was supported by the Office of Advanced Cyberinfrastructure of the National Science Foundation under Grant Nos. OAC-2103717 and OAC- 2401207.

AUTHOR DECLARATIONS

Conflict of Interest

The authors have no conflicts to disclose.

Author Contributions

Chiara Aieta: Conceptualization (equal); Data curation (equal); Formal analysis (equal); Investigation (equal); Methodology (equal); Software (equal); Validation (equal); Visualization (equal); Writing – original draft (equal). **Scott M. Garner**: Investigation (equal); Methodology (equal); Software (equal); Writing – review & editing (equal). **Aodong Liu**: Investigation (equal); Methodology (equal); Software (equal); Writing – review & editing (equal). **Xiaosong Li**: Investigation (equal); Methodology (equal); Software (equal); Writing – review & editing (equal). **Sharon Hammes-Schiffer**: Conceptualization (equal); Funding acquisition (equal); Investigation (equal); Methodology (equal); Project administration (equal);

Resources (equal); Supervision (equal); Writing – review & editing (equal).

DATA AVAILABILITY

The data that support the findings of this study are openly available in Zenodo at https://doi.org/10.5281/zenodo.18381251.

REFERENCES

[1]E. Ditler and S. Luber, "Vibrational spectroscopy by means of first-principles molecular dynamics simulations," Wiley Interdiscip. Rev.: Comput. Mol. Sci. **12**, e1605 (2022).

[2]G. Mathias, S. D. Ivanov, A. Witt, M. D. Baer, and D. Marx, "Infrared spectroscopy of fluxional molecules from (ab initio) molecular dynamics: Resolving large-amplitude motion, multiple conformations, and permutational symmetries," J. Chem. Theory Comput. **8**, 224–234 (2012).

[3]S. C. Althorpe, "Path integral simulations of condensed-phase vibrational spectroscopy," Annu. Rev. Phys. Chem. **75**, 397–420 (2024).

[4]T. Plé, S. Huppert, F. Finocchi, P. Depondt, and S. Bonella, "Anharmonic spectral features via trajectory-based quantum dynamics: A perturbative analysis of the interplay between dynamics and sampling," J. Chem. Phys. **155**, 104108 (2021).

[5]R. Conte, C. Aieta, M. Cazzaniga, and M. Ceotto, "A perspective on the investigation of spectroscopy and kinetics of complex molecular systems with semiclassical approaches," J. Phys. Chem. Lett. **15**, 7566–7576 (2024).

[6]M. Basire, F. Mouhat, G. Fraux, A. Bordage, J.-L. Hazemann, M. Louvel, R. Spezia, S. Bonella, and R. Vuilleumier, "Fermi resonance in CO_2: Mode assignment and quantum nuclear effects from first principles molecular dynamics," J. Chem. Phys. **146**, 134102 (2017).

[7]J. M. Bowman, S. Carter, and X. Huang, "Multimode: A code to calculate rovibrational energies of polyatomic molecules," Int. Rev. Phys. Chem. **22**, 533–549 (2003).

[8]T. Mathea and G. Rauhut, "Assignment of vibrational states within configuration interaction calculations," J. Chem. Phys. **152**, 194112 (2020).

[9]V. Barone, M. Biczysko, J. Bloino, M. Borkowska-Panek, I. Carnimeo, and P. Panek, "Toward anharmonic computations of vibrational spectra for large molecular systems," Int. J. Quantum Chem. **112**, 2185–2200 (2012).

[10]P. R. Franke, J. F. Stanton, and G. E. Douberly, "How to VPT2: Accurate and intuitive simulations of CH stretching infrared spectra using VPT2+K with large effective Hamiltonian resonance treatments," J. Phys. Chem. A **125**, 1301–1324 (2021).

[11]H.-D. Meyer, U. Manthe, and L. S. Cederbaum, "The multi-configurational time-dependent Hartree approach," Chem. Phys. Lett. **165**, 73–78 (1990).

[12]H.-D. Meyer, M. Schröder, and O. Vendrell, "Vibrational spectra of flexible systems using the MCTDH approach," in *Vibrational Dynamics of Molecules* (World Scientific Press, 2022), pp. 340–377.

[13]A. Witt, S. D. Ivanov, M. Shiga, H. Forbert, and D. Marx, "On the applicability of centroid and ring polymer path integral molecular dynamics for vibrational spectroscopy," J. Chem. Phys. **130**, 194510 (2009).

[14]I. R. Craig and D. E. Manolopoulos, "Quantum statistics and classical mechanics: Real time correlation functions from ring polymer molecular dynamics," J. Chem. Phys. **121**, 3368–3373 (2004).

[15]S. Jang and G. A. Voth, "A derivation of centroid molecular dynamics and other approximate time evolution methods for path integral centroid variables," J. Chem. Phys. **111**, 2371–2384 (1999).

[16]W. H. Miller, "The semiclassical initial value representation: A potentially practical way for adding quantum effects to classical molecular dynamics simulations," J. Phys. Chem. A **105**, 2942–2955 (2001).

[17]X. Sun, H. Wang, and W. H. Miller, "On the semiclassical description of quantum coherence in thermal rate constants," J. Chem. Phys. **109**, 4190–4200 (1998).

[18]S. Malpathak and N. Ananth, "Semiclassical dynamics in Wigner phase space I: Adiabatic hybrid Wigner dynamics," J. Chem. Phys. **161**, 094109 (2024).

[19]F. Grossmann, "A semiclassical hybrid approach to linear response functions for infrared spectroscopy," Phys. Scr. **91**, 044004 (2016).

[20]M. Ceotto, S. Atahan, G. F. Tantardini, and A. Aspuru-Guzik, "Multiple coherent states for first-principles semiclassical initial value representation molecular dynamics," J. Chem. Phys. **130**, 234113 (2009).

[21]C. Aieta, M. Cazzaniga, D. Moscato, C. Lanzi, L. Bocchi, M. M. Costanza, M. Ceotto, and R. Conte, "Quantum dynamics through a handful of semiclassical trajectories," Rend. Lincei Sci. Fis. Nat. **36**, 445–455 (2025).

[22]R. Conte, G. Mandelli, G. Botti, D. Moscato, C. Lanzi, M. Cazzaniga, C. Aieta, and M. Ceotto, "Semiclassical description of nuclear quantum effects in solvated and condensed phase molecular systems," Chem. Sci. **16**, 20–28 (2025).

[23]S. P. Webb, T. Iordanov, and S. Hammes-Schiffer, "Multiconfigurational nuclear-electronic orbital approach: Incorporation of nuclear quantum effects in electronic structure calculations," J. Chem. Phys. **117**, 4106–4118 (2002).

[24]F. Pavošević, T. Culpitt, and S. Hammes-Schiffer, "Multicomponent quantum chemistry: Integrating electronic and nuclear quantum effects via the nuclear–electronic orbital method," Chem. Rev. **120**, 4222–4253 (2020).

[25]S. Hammes-Schiffer, "Nuclear–electronic orbital methods: Foundations and prospects," J. Chem. Phys. **155**, 030901 (2021).

[26]M. V. Pak, A. Chakraborty, and S. Hammes-Schiffer, "Density functional theory treatment of electron correlation in the nuclear-electronic orbital approach," J. Phys. Chem. A **111**, 4522–4526 (2007).

[27]Y. Yang, K. R. Brorsen, T. Culpitt, M. V. Pak, and S. Hammes-Schiffer, "Development of a practical multicomponent density functional for electron-proton correlation to produce accurate proton densities," J. Chem. Phys. **147**, 114113 (2017).

[28]K. R. Brorsen, Y. Yang, and S. Hammes-Schiffer, "Multicomponent density functional theory: Impact of nuclear quantum effects on proton affinities and geometries," J. Phys. Chem. Lett. **8**, 3488–3493 (2017).

[29]Y. Yang, T. Culpitt, and S. Hammes-Schiffer, "Multicomponent time-dependent density functional theory: Proton and electron excitation energies," J. Phys. Chem. Lett. **9**, 1765–1770 (2018).

[30]T. Culpitt, Y. Yang, F. Pavošević, Z. Tao, and S. Hammes-Schiffer, "Enhancing the applicability of multicomponent time-dependent density functional theory," J. Chem. Phys. **150**, 201101 (2019).

[31]C. L. Malbon and S. Hammes-Schiffer, "Nuclear-electronic orbital multireference configuration interaction for ground and excited vibronic states and fundamental insights into multicomponent basis sets," J. Chem. Theory Comput. **21**, 3968–3980 (2025).

[32]R. J. Stein, C. L. Malbon, and S. Hammes-Schiffer, "Computing hydrogen tunneling splittings with nuclear-electronic orbital multireference configuration interaction," J. Phys. Chem. Lett. **16**, 7718–7724 (2025).

[33]F. Pavošević, T. Culpitt, and S. Hammes-Schiffer, "Multicomponent coupled cluster singles and doubles theory within the nuclear-electronic orbital framework," J. Chem. Theory Comput. **15**, 338–347 (2018).

[34]Y. Yang, P. E. Schneider, T. Culpitt, F. Pavošević, and S. Hammes-Schiffer, "Molecular vibrational frequencies within the nuclear–electronic orbital framework," J. Phys. Chem. Lett. **10**, 1167–1172 (2019).

[35]T. Culpitt, Y. Yang, P. E. Schneider, F. Pavošević, and S. Hammes-Schiffer, "Molecular vibrational frequencies with multiple quantum protons within the nuclear-electronic orbital framework," J. Chem. Theory Comput. **15**, 6840–6849 (2019).

[36]X. Xu and Y. Yang, "Molecular vibrational frequencies from analytic hessian of constrained nuclear–electronic orbital density functional theory," J. Chem. Phys. **154**, 244110 (2021).

[37]X. Xu, Z. Chen, and Y. Yang, "Molecular dynamics with constrained nuclear electronic orbital density functional theory: Accurate vibrational spectra from efficient incorporation of nuclear quantum effects," J. Am. Chem. Soc. **144**, 4039–4046 (2022).

[38]Y. Zhang, Y. Wang, X. Xu, Z. Chen, and Y. Yang, "Vibrational spectra of highly anharmonic water clusters: Molecular dynamics and harmonic analysis revisited with constrained nuclear-electronic orbital methods," J. Chem. Theory Comput. **19**, 9358–9368 (2023).

[39]Z. Chen and Y. Yang, "Incorporating nuclear quantum effects in molecular dynamics with a constrained minimized energy surface," J. Phys. Chem. Lett. **14**, 279–286 (2023).
[40]J. Langford, Y. Zhang, Z. Chen, and Y. Yang, "Where is the hidden intramolecular H-bonding vibrational signal in the proline matrix IR spectrum?," J. Chem. Phys. **161**, 134302 (2024).
[41]Z. Liu, Y. Wang, Y. Zhang, N. Yang, and Y. Yang, "Characterizing infrared spectra of $OH^- \cdot (H_2O)_2$ and $OH^- \cdot (H_2O)_3$ with constrained nuclear-electronic orbital molecular dynamics," J. Phys. Chem. A **129**, 9883 (2025).
[42]L. Zhao, Z. Tao, F. Pavosìevicì, A. Wildman, S. Hammes-Schiffer, and X. Li, "Real-time time-dependent nuclear-electronic orbital approach: Dynamics beyond the Born–Oppenheimer approximation," J. Phys. Chem. Lett. **11**, 4052–4058 (2020).
[43]L. Zhao, A. Wildman, Z. Tao, P. Schneider, S. Hammes-Schiffer, and X. Li, "Nuclear–electronic orbital Ehrenfest dynamics," J. Chem. Phys. **153**, 224111 (2020).
[44]L. Zhao, A. Wildman, F. Pavošević, J. C. Tully, S. Hammes-Schiffer, and X. Li, "Excited state intramolecular proton transfer with nuclear-electronic orbital Ehrenfest dynamics," J. Phys. Chem. Lett. **12**, 3497–3502 (2021).
[45]T. E. Li and S. Hammes-Schiffer, "Electronic Born-Oppenheimer approximation in nuclear-electronic orbital dynamics," J. Chem. Phys. **158**, 114118 (2023).
[46]J. Xu, R. Zhou, T. E. Li, S. Hammes-Schiffer, and Y. Kanai, "Lagrangian formulation of nuclear–electronic orbital Ehrenfest dynamics with real-time TDDFT for extended periodic systems," J. Chem. Phys. **161**, 194109 (2024).
[47]T. E. Li, X. Li, and S. Hammes-Schiffer, "Energy conservation in real-time nuclear–electronic orbital Ehrenfest dynamics," J. Chem. Phys. **162**, 144106 (2025).
[48]A. Rognoni, R. Conte, and M. Ceotto, "Caldeira–Leggett model vs ab initio potential: A vibrational spectroscopy test of water solvation," J. Chem. Phys. **154**, 094106 (2021).
[49]J. J. Goings, P. J. Lestrange, and X. Li, "Real-time time-dependent electronic structure theory," Wiley Interdiscip. Rev.: Comput. Mol. Sci. **8**, e1341 (2018).
[50]J. B. Keller, "Corrected Bohr-Sommerfeld quantum conditions for nonseparable systems," Ann. Phys. **4**, 180–188 (1958).
[51]C. C. Martens and G. S. Ezra, "EBK quantization of nonseparable systems: A Fourier transform method," J. Chem. Phys. **83**, 2990–3001 (1985).
[52]D. G. Trhular and J. T. Muckerman, "Reactive scattering cross sections III: Quasiclassical and semiclassical method," in *Atom-Molecule Collision Theory: A Guide for the Experimentalist* (Plenum Press, New York, 1979), pp. 505–566.
[53]M. Paranjothy, R. Sun, Y. Zhuang, and W. L. Hase, "Direct chemical dynamics simulations: Coupling of classical and quasiclassical trajectories with electronic structure theory," Wiley Interdiscip. Rev.: Comput. Mol. Sci. **3**, 296–316 (2013).
[54]R. Conte, C. Aieta, G. Botti, M. Cazzaniga, M. Gandolfi, C. Lanzi, G. Mandelli, D. Moscato, and M. Ceotto, "Anharmonicity and quantum nuclear effects in theoretical vibrational spectroscopy: A molecular tale of two cities," Theor. Chem. Acc. **142**, 53 (2023).
[55]G. Botti, M. Ceotto, and R. Conte, "Investigating the spectroscopy of the gas phase guanine–cytosine pair: Keto versus enol configurations," J. Phys. Chem. Lett. **14**, 8940–8947 (2023).
[56]T. L. Fischer, M. Bödecker, S. M. Schweer, J. Dupont, V. Lepère, A. Zehnacker-Rentien, M. A. Suhm, B. Schröder, T. Henkes, D. M. Andrada *et al.*, "The first hydra challenge for computational vibrational spectroscopy," Phys. Chem. Chem. Phys. **25**, 22089–22102 (2023).
[57]D. Moscato, F. Gabas, R. Conte, and M. Ceotto, "Vibrational spectroscopy simulation of solvation effects on a G-quadruplex," J. Biomol. Struct. Dyn. **41**, 14248–14258 (2023).
[58]W. H. Miller, W. L. Hase, and C. L. Darling, "A simple model for correcting the zero point energy problem in classical trajectory simulations of polyatomic molecules," J. Chem. Phys. **91**, 2863–2868 (1989).
[59]J. M. Bowman, B. Gazdy, and Q. Sun, "A method to constrain vibrational energy in quasiclassical trajectory calculations," J. Chem. Phys. **91**, 2859 (1989).
[60]G. Czako, A. L. Kaledin, and J. M. Bowman, "A practical method to avoid zero-point leak in molecular dynamics calculations: Application to the water dimer," J. Chem. Phys. **132**, 164103 (2010).
[61]A. Bruner, D. LaMaster, and K. Lopata, "Accelerated broadband spectra using transition dipole decomposition and Padé approximants," J. Chem. Theory Comput. **12**, 3741–3750 (2016).
[62]C. Qu and J. M. Bowman, "Revisiting adiabatic switching for initial conditions in quasi-classical trajectory calculations: Application to CH_4," J. Phys. Chem. A **120**, 4988–4993 (2016).
[63]T. Nagy and G. Lendvay, "Adiabatic switching extended to prepare semiclassically quantized rotational–vibrational initial states for quasiclassical trajectory calculations," J. Phys. Chem. Lett. **8**, 4621–4626 (2017).
[64]J. Huang, J. J. Valentini, and J. T. Muckerman, "Sampling of semiclassically quantized polyatomic molecule vibrations by an adiabatic switching method: Application to quasiclassical trajectory calculations," J. Chem. Phys. **102**, 5695–5707 (1995).
[65]E. Epifanovsky, A. T. B. Gilbert, X. Feng, J. Lee, Y. Mao, N. Mardirossian, P. Pokhilko, A. F. White, M. P. Coons, A. L. Dempwolff, Z. Gan, D. Hait, P. R. Horn, L. D. Jacobson, I. Kaliman, J. Kussmann, A. W. Lange, K. U. Lao, D. S. Levine, J. Liu, S. C. McKenzie, A. F. Morrison, K. D. Nanda, F. Plasser, D. R. Rehn, M. L. Vidal, Z.-Q. You, Y. Zhu, B. Alam, B. J. Albrecht, A. Aldossary, E. Alguire, J. H. Andersen, V. Athavale, D. Barton, K. Begam, A. Behn, N. Bellonzi, Y. A. Bernard, E. J. Berquist, H. G. A. Burton, A. Carreras, K. Carter-Fenk, R. Chakraborty, A. D. Chien, K. D. Closser, V. Cofer-Shabica, S. Dasgupta, M. de Wergifosse, J. Deng, M. Diedenhofen, H. Do, S. Ehlert, P.-T. Fang, S. Fatehi, Q. Feng, T. Friedhoff, J. Gayvert, Q. Ge, G. Gidofalvi, M. Goldey, J. Gomes, C. E. González-Espinoza, S. Gulania, A. O. Gunina, M. W. D. Hanson-Heine, P. H. P. Harbach, A. Hauser, M. F. Herbst, M. Hernández Vera, M. Hodecker, Z. C. Holden, S. Houck, X. Huang, K. Hui, B. C. Huynh, M. Ivanov, Á. Jász, H. Ji, H. Jiang, B. Kaduk, S. Kähler, K. Khistyaev, J. Kim, G. Kis, P. Klunzinger, Z. Koczor-Benda, J. H. Koh, D. Kosenkov, L. Koulias, T. Kowalczyk, C. M. Krauter, K. Kue, A. Kunitsa, T. Kus, I. Ladjánszki, A. Landau, K. V. Lawler, D. Lefrancois, S. Lehtola, R. R. Li, Y.-P. Li, J. Liang, M. Liebenthal, H.-H. Lin, Y.-S. Lin, F. Liu, K.-Y. Liu, M. Loipersberger, A. Luenser, A. Manjanath, P. Manohar, E. Mansoor, S. F. Manzer, S.-P. Mao, A. V. Marenich, T. Markovich, S. Mason, S. A. Maurer, P. F. McLaughlin, M. F. S. J. Menger, J.-M. Mewes, S. A. Mewes, P. Morgante, J. W. Mullinax, K. J. Oosterbaan, G. Paran, A. C. Paul, S. K. Paul, F. Pavošević, Z. Pei, S. Prager, E. I. Proynov, Á. Rák, E. Ramos-Cordoba, B. Rana, A. E. Rask, A. Rettig, R. M. Richard, F. Rob, E. Rossomme, T. Scheele, M. Scheurer, M. Schneider, N. Sergueev, S. M. Sharada, W. Skomorowski, D. W. Small, C. J. Stein, Y.-C. Su, E. J. Sundstrom, Z. Tao, J. Thirman, G. J. Tornai, T. Tsuchimochi, N. M. Tubman, S. P. Veccham, O. Vydrov, J. Wenzel, J. Witte, A. Yamada, K. Yao, S. Yeganeh, S. R. Yost, A. Zech, I. Y. Zhang, X. Zhang, Y. Zhang, D. Zuev, A. Aspuru-Guzik, A. T. Bell, N. A. Besley, K. B. Bravaya, B. R. Brooks, D. Casanova, J.-D. Chai, S. Coriani, C. J. Cramer, G. Cserey, A. E. DePrince III, R. A. DiStasio, Jr., A. Dreuw, B. D. Dunietz, T. R. Furlani, W. A. Goddard III, S. Hammes-Schiffer, T. Head-Gordon, W. J. Hehre, C.-P. Hsu, T.-C. Jagau, Y. Jung, A. Klamt, J. Kong, D. S. Lambrecht, W. Liang, N. J. Mayhall, C. W. McCurdy, J. B. Neaton, C. Ochsenfeld, J. A. Parkhill, R. Peverati, V. A. Rassolov, Y. Shao, L. V. Slipchenko, T. Stauch, R. P. Steele, J. E. Subotnik, A. J. W. Thom, A. Tkatchenko, D. G. Truhlar, T. Van Voorhis, T. A. Wesolowski, K. B. Whaley, H. L. Woodcock III, P. M. Zimmerman, S. Faraji, P. M. W. Gill, M. Head-Gordon, J. M. Herbert, A. I. Krylov, P. M. W. Gill, M. Head-Gordon, J. M. Herbert, and A. I. Krylov, "Software for the frontiers of quantum chemistry: An overview of developments in the Q-Chem 5 package," J. Chem. Phys. **155**, 084801 (2021).
[66]A. D. Becke, "Density-functional thermochemistry. III. The role of exact exchange," J. Chem. Phys. **98**, 5648–5652 (1993).
[67]C. Adamo and V. Barone, "Toward reliable density functional methods without adjustable parameters: The PBE0 model," J. Chem. Phys. **110**, 6158–6170 (1999).
[68]J.-D. Chai and M. Head-Gordon, "Systematic optimization of long-range corrected hybrid density functionals," J. Chem. Phys. **128**, 084106 (2008).
[69]T. H. Dunning, Jr., "Gaussian basis sets for use in correlated molecular calculations. I. The atoms boron through neon and hydrogen," J. Chem. Phys. **90**, 1007–1023 (1989).

[70]Q. Yu, F. Pavošević, and S. Hammes-Schiffer, "Development of nuclear basis sets for multicomponent quantum chemistry methods," J. Chem. Phys. **152**, 244123 (2020).
[71]D. B. Williams-Young, A. Petrone, S. Sun, T. F. Stetina, P. Lestrange, C. E. Hoyer, D. R. Nascimento, L. Koulias, A. Wildman, J. Kasper, J. J. Goings, F. Ding, A. E. DePrince III, E. F. Valeev, and X. Li, "The chronus quantum software package," Wiley Interdiscip. Rev.: Comput. Mol. Sci. **10**, e1436 (2020).
[72]A. Liu, M. Chow, A. Wildman, M. J. Frisch, S. Hammes-Schiffer, and X. Li, "Simultaneous optimization of nuclear–electronic orbitals," J. Phys. Chem. A **126**, 7033–7039 (2022).
[73]X. Li, J. C. Tully, H. B. Schlegel, and M. J. Frisch, "*Ab initio* Ehrenfest dynamics," J. Chem. Phys. **123**, 084106 (2005).
[74]X. Li, S. M. Smith, A. N. Markevitch, D. A. Romanov, R. J. Levis, and H. B. Schlegel, "A time-dependent Hartree–Fock approach for studying the electronic optical response of molecules in intense fields," Phys. Chem. Chem. Phys. **7**, 233–239 (2005).
[75]National Institute of Standards and Technology (NIST), "Formic acid infrared spectrum," (2025); https://webbook.nist.gov/cgi/cbook.cgi?ID=C64186&Type=IR-SPEC&Index=1 (accessed 01 10 2025).
[76]R. C. Millikan and K. S. Pitzer, "Infrared spectra and vibrational assignment of monomeric formic acid," J. Chem. Phys. **27**, 1305–1308 (1957).
[77]H. K. Gerardi, A. F. DeBlase, X. Su, K. D. Jordan, A. B. McCoy, and M. A. Johnson, "Unraveling the anomalous solvatochromic response of the formate ion vibrational spectrum: An infrared, Ar-tagging study of the HCO_2^-, DCO_2^-, and $HCO_2^- \cdot H_2O$ ions," J. Phys. Chem. Lett. **2**, 2437–2441 (2011).
[78]E. M. Myshakin, K. D. Jordan, E. L. Sibert III, and M. A. Johnson, "Large anharmonic effects in the infrared spectra of the symmetrical $CH_3NO_2^- \cdot (H_2O)$ and $CH_3CO_2^- \cdot (H_2O)$ complexes," J. Chem. Phys. **119**, 10138–10145 (2003).
[79]W. H. Robertson, E. A. Price, J. M. Weber, J.-W. Shin, G. H. Weddle, and M. A. Johnson, "Infrared signatures of a water molecule attached to triatomic domains of molecular anions: Evolution of the H-bonding configuration with domain length," J. Phys. Chem. A **107**, 6527–6532 (2003).
[80]N. Heine, E. G. Kratz, R. Bergmann, D. P. Schofield, K. R. Asmis, K. D. Jordan, and A. B. McCoy, "Vibrational spectroscopy of the water–nitrate complex in the O–H stretching region," J. Phys. Chem. A **118**, 8188–8197 (2014).
[81]B. V. Henderson and K. D. Jordan, "One-dimensional adiabatic model approach for calculating progressions in vibrational spectra of ion–water complexes," J. Phys. Chem. A **123**, 7042–7050 (2019).
[82]E. V. Henderson and K. D. Jordan, "Two-dimensional adiabatic model for calculating progressions resulting from stretch–rock coupling in vibrational spectra of anion–water complexes," J. Phys. Chem. Lett. **12**, 6326–6329 (2021).
[83]P. Hamm and G. Stock, "Nonadiabatic vibrational dynamics in the $HCO_2^- \cdot H_2O$ complex," J. Chem. Phys. **143**, 134308 (2015).
[84]M. L. Laury, M. J. Carlson, and A. K. Wilson, "Vibrational frequency scale factors for density functional theory and the polarization consistent basis sets," J. Comput. Chem. **33**, 2380–2387 (2012).
[85]M. Micciarelli, F. Gabas, R. Conte, and M. Ceotto, "An effective semiclassical approach to IR spectroscopy," J. Chem. Phys. **150**, 184113 (2019).